Title

Fatty acid–binding protein 4 downregulation drives calcification in the development of kidney stone disease

Journal

Kidney International, 97(5)

ISSN

0085-2538

Authors

Taguchi, Kazumi
Chen, Ling
Usawachintachit, Manint
et al.

Publication Date

2020-05-01

DOI

10.1016/j.kint.2020.01.042

Peer reviewed

Fatty acid–binding protein 4 downregulation drives calcification in the development of kidney stone disease

Kazumi Taguchi[1,2], Ling Chen[4], Manint Usawachintachit[1,3], Shuzo Hamamoto[2], Misun Kang[4], Teruaki Sugino[2], Rei Unno[2], David T. Tzou[1], Benjamin A. Sherer[1], Atsushi Okada[2], Takahiro Yasui[2], Sunita P. Ho[4], Marshall L. Stoller[1] and Thomas Chi[1]

[1]Department of Urology, University of California, San Francisco, California, USA; [2]Department of Nephro-urology, Nagoya City University Graduate School of Medical Sciences, Nagoya, Japan; [3]Division of Urology, Faculty of Medicine, Chulalongkorn University, King Chulalongkorn Memorial Hospital, The Thai Red Cross Society, Bangkok, Thailand; and [4]Division of Biomaterials and Bioengineering, Department of Preventive and Restorative Dental Sciences, University of California San Francisco, San Francisco, California, USA

Nephrolithiasis is a significant source of morbidity, and its incidence has increased significantly over the last decades. This rise has been attributed to concurrent increasing rates of obesity, associated with a 3-time risk of developing NL. To date, the mechanism by which obesity is linked to stone formation has not been elucidated. We aimed to utilize a transcriptomics approach to discover the missing link between these two epidemic diseases. We investigated gene expression profiling of nephrolithiasis patients by two RNA-sequencing approaches: comparison between renal papilla tissue with and without the presence of calcified Randall's plaques (RP), and comparison between the papilla, medulla, and cortex regions from within a single recurrent stone forming kidney. Results were overlaid between differently expressed genes found in the patient cohort and in the severely lithogenic kidney to identify common genes. Overlay of these two RNA-sequencing datasets demonstrated there is impairment of lipid metabolism in renal papilla tissue containing RP linked to downregulation of *fatty acid binding protein (FABP) 4*. Immunohistochemistry of human kidney specimens and microarray analysis of renal tissue from a nephrolithiasis mouse model confirmed that *FABP4* downregulation is associated with renal stone formation. In a *FABP4* knockout mouse model, *FABP4* deficiency resulted in development of both renal and urinary crystals. Our study revealed that *FABP4* plays an important, previously unrecognized role in kidney stone formation, providing a feasible mechanism to explain the link between nephrolithiasis and metabolic syndrome.

Kidney International (2020) **97,** 1042–1056; https://doi.org/10.1016/j.kint.2020.01.042

KEYWORDS: fatty acid–binding protein; kidney stone; metabolic syndrome; Randall's plaque; RNA-sequence

Correspondence: *Thomas Chi, Department of Urology, University of California, San Francisco, 400 Parnassus Ave., Sixth Floor, Suite A610, San Francisco, CA 94143. E-mail: tom.chi@ucsf.edu*

Received 28 March 2019; revised 23 January 2020; accepted 30 January 2020; published online 29 February 2020

Kidney stone disease has a high prevalence worldwide, ranging up to 13% in North America, 9% in Europe, and 5% in Asia.[1] They are painful for patients, often lead to surgery, and impart a significant economic impact.[2] Many have reported nephrolithiasis (NL) to be associated with the metabolic syndrome (MetS),[3,4] but the mechanism by which they are linked is not understood.[5] This poorly characterized association affords an opportunity to identify new targets that may lead to medical prevention of recurrence of kidney stones.

Numerous lines of evidence support that gene mutations, variants, and single nucleotide polymorphism are associated with the development of calcium stones.[6] Our previous microarray study demonstrated that comparative gene expression profiling of renal papilla tissue with or without calcified Randall's plaques (RP) (calcium deposits in the renal papilla thought to be precursor lesions to kidney stones) revealed that renal cell injury, oxidative stress, and sodium/potassium transporters contribute to the development of RP in the tip of the papilla.[7] This comparative transcriptomics approach provided discovery of newly identified genes possibly associated with the stone-formation process. We have also demonstrated the importance of mixing pressure and chemical gradients, both in renal tubules and vessels, between the medulla and papilla for the formation of RP.[8] Coupled together, these studies previously suggested that histologic and transcriptomic investigation of kidney tissue at the level of the papilla is necessary to better understand the molecular pathogenesis of kidney stone disease. The transition of transcriptomics research tools from microarray to RNA-sequencing (RNA-Seq)[9] creates the opportunity for more granular examination of genes that may contribute to progression of kidney stone disease.[10] Although RNA-Seq performed on blood samples has been used to profile monogenic causes of urinary stone formation in young patients with NL,[11] investigation using human kidney tissue has yet to be undertaken.

To elucidate lithogenic genes associated with the formation of kidney stones, we investigated the gene-expression profile of different regions of the kidney from 1 human subject with

Table 1 | Clinical history for each subject with renal papillary biopsy

Age at surgery, yr	Sex	Ethnicity	Age at first stone episode, yr	HTN	HLP	DM	BMI, kg/m^2	eGFR, ml/min per 1.73 m^2	Stone component		Stone location	Stone diameter, mm	Hydronephrosis
									CaOx, %	CaP, %			
40	Male	Japanese	40	–	–	–	27.8	82.0	87	13	Proximal ureter	10	Mild
74	Male	Japanese	70	+	–	+	20.5	47.3	100		Renal pelvis	8	None
47	Female	Japanese	38	–	–	+	33.8	94.2	95	5	Renal pelvis	23	Mild
45	Male	Asian American	45	–	+	–	31.5	79.2	80	20	Proximal ureter	12	Moderate
46	Male	African American	46	–	–	–	36.0	82.7	100		Renal pelvis	14	None
38	Female	Hispanic or Latino	30	–	–	–	25.2	64.6	100		Renal pelvis	42	None
49	Female	Hispanic or Latino	49	–	–	–	48.8	79.4	65	35	Renal pelvis	15	None
40	Female	White	33	–	–	–	44.1	80.6	100		Distal ureter	4	None
46	Female	White	46	–	–	–	34.2	63.6	65	35	Renal pelvis	20	Mild
32	Female	Asian American	25	–	+	–	20.9	50.2	85	15	Renal pelvis	34	None
58	Male	Asian American	58	+	+	–	31.4	80.0	100		Distal ureter	4	Mild
67	Male	White	67	–	–	–	28.1	66.3	85	15	Proximal ureter	12	Moderate

+, positive history of this complication; –, absence of a history of this complication; BMI, body mass index; Ca, calcium; CaOx, calcium oxalate; CaP, calcium phosphate; Cit, citrate; DM, diabetes mellitus; eGFR, estimated glomerular filtration rate; HLP, hyperlipidemia; HTN, hypertension.

severe recurrent urinary stone disease and compared these results with expression profiles taken from a larger sample of renal papilla biopsies acquired from multiple stone-forming subjects. Gene hits were confirmed with immunohistochemical staining and validated in murine models.

RESULTS

Gene expression profiles differ in stone-forming regions of renal papilla tissue

We obtained a pair of samples (1 plaque and 1 nonplaque endoscopic renal papillary biopsy) from consecutive patients with pure or predominantly calcium oxalate (CaOx) stones who had undergone endoscopic stone removal. Among 30 samples from 15 patients, a total of 24 samples, consisting of 12 pairs of plaque and nonplaque papillae from 12 patients, were of sufficient quality for analysis as determined by quality screening.[12] These included 3 Japanese, 3 Asian American, 3 white American, 2 Hispanic/Latino American, and 1 Black American subjects. Patient clinical history, as well as serum studies and urinary chemistries, are summarized in Tables 1 and 2.

RNA-Seq provided transcriptomic expression patterns for these papilla tissue samples, and papillae containing RP and those without plaques were compared to identify genes related to plaque formation. Fourteen genes showed significantly higher expression levels and 9 genes lower expression levels in plaque-containing papilla tissue compared with nonplaque-containing papilla tissue (Supplementary Table S1). Fold changes varied between 0.50 and 2.09, with less than a 0.1 false discovery rate (FDR). Ingenuity Pathway Analysis (IPA, QIAGEN, Hilden, Germany) network analysis revealed that this gene set was associated with the functional categories of endocrine system, lipid metabolism, small-molecule biochemistry, gastrointestinal disease, hepatic-system disease, and organismal injury and abnormalities (Supplementary Figure S1). In addition, the top 5 hits for disease and function analysis by IPA demonstrated that fatty acid–binding protein 4 (FABP4), leptin, purinergic receptor P2X2, and somatostatin were mainly associated with the differences between plaque- and nonplaque-containing papilla via the following disease or functional categories: release of fatty acid/L-glutamic acid, size of fat pad, glycogenolysis, and quantity of monounsaturated fatty acids (Table 3).

Clustering heatmap analysis of differentially expressed genes between plaque and nonplaque papillary tissue samples demonstrated no influence of ethnicity on gene clustering. Gene expression pattern appeared to distinguish plaque from nonplaque areas of the kidneys (Figure 1).

Renal papilla tissue demonstrates distinctive gene-expression patterns compared with the medulla and cortex

We then performed RNA-Seq to characterize the differences among the cortex, medulla, and papilla from needle-core

Table 2 | Serum studies and urinary chemistries of subjects with papillary biopsies[a]

Source	Value	Normal range[b]
Serum test		
Hematocrit, %	41.6 (3.4)	40.7–50.1
Ca, mg/dl	9.20 (0.26)	8.8–10.1
Cre, mg/dl	0.90 (0.15)	0.65–1.07
Urine test		
pH	5.94 [5.59, 6.27]	4.5–7.5
Volume, L	1.50 [1.34, 1.67]	
Ca, mg/d	296 [263, 334]	100–300
Phosphorus, g/d	0.90 [0.79, 1.03]	0.5–1.0
Sodium, mmol/d	214 [189, 229]	70–250
Potassium, mmol/d	57.5 [52.8, 62.8]	25.0–100.0
Chloride, mmol/d	214 [191, 226]	70–250
Magnesium, mg/d	103 [95, 113]	0–100
Oxalate, mg/d	34.0 [24.4, 41.8]	10.3–41.5
Citrate, mg/d	493 [373, 768]	138–1010
Cr, g/d	1.62 [1.56, 2.01]	0.50–1.50

Ca, calcium; Cr, creatinine.
[a]Data were available from 8 patients for serum studies and 4 patients for urine chemistries.
[b]Ranges are described as institutional standards.
Values are presented as mean (SD), or median [interquartile range].

Table 3 | Disease and function analysis of differentially expressed genes between plaque and nonplaque papilla tissue

Categories	Diseases or functions annotation	*P* value	Molecules (direction)
Lipid metabolism, molecular transport, small-molecule biochemistry	Release of fatty acid	0.0000542	FABP4(↓), LEP(↓), P2RX2(↑), SST(↓)
Connective-tissue development and function, tissue morphology	Size of fat pad	0.0000735	FABP4(↓), LEP(↓)
Amino-acid metabolism, cell-to-cell signaling and interaction, molecular transport, small-molecule biochemistry	Release of L-glutamic acid	0.0000862	LEP(↓), P2RX2(↑), SST(↓)
Carbohydrate metabolism	Glycogenolysis	0.0000868	LEP(↓), SST(↓)
Lipid metabolism, molecular transport, small-molecule biochemistry	Quantity of monounsaturated fatty acids	0.000133	FABP4(↓), LEP(↓)
Endocrine-system disorders, gastrointestinal disease, metabolic disease, organismal injury and abnormalities	Gestational diabetes mellitus	0.00019	FABP4(↓), LEP(↓)
Cellular function and maintenance	Hyperpolarization of neurons	0.00019	LEP(↓), SST(↓)
Lipid metabolism, molecular transport, small-molecule biochemistry	Quantity of non-esterified fatty acid	0.00019	FABP4(↓), LEP(↓)
Lipid metabolism, molecular transport, small-molecule biochemistry	Accumulation of cholesterol ester	0.000256	FABP4(↓), LEP(↓)
Amino-acid metabolism, lipid metabolism, molecular transport, small- molecule biochemistry	Release of GABA	0.000305	P2RX2(↑), SST(↓)

↓, downregulation; ↑, upregulation; FABP4, fatty acid–binding protein 4; GABA, gamma-aminobutyric acid; LEP, leptin; P2RX2, purinergic receptor P2X 2; SST, somatostatin.

biopsy specimens from a recurrent CaOx stone-forming kidney. Tissue was obtained from a structurally normal kidney removed for severe, unilateral renal stone formation in a 23-year-old man who elected nephrectomy for debilitating stone disease. Immediately after kidney removal, needle-core tissue biopsies were taken from the kidney and divided into 3 regions (papilla [n = 4], medulla [n = 4], and cortex [n = 4]) (Supplementary Figure S2); 5871, 436, and 356 differentially

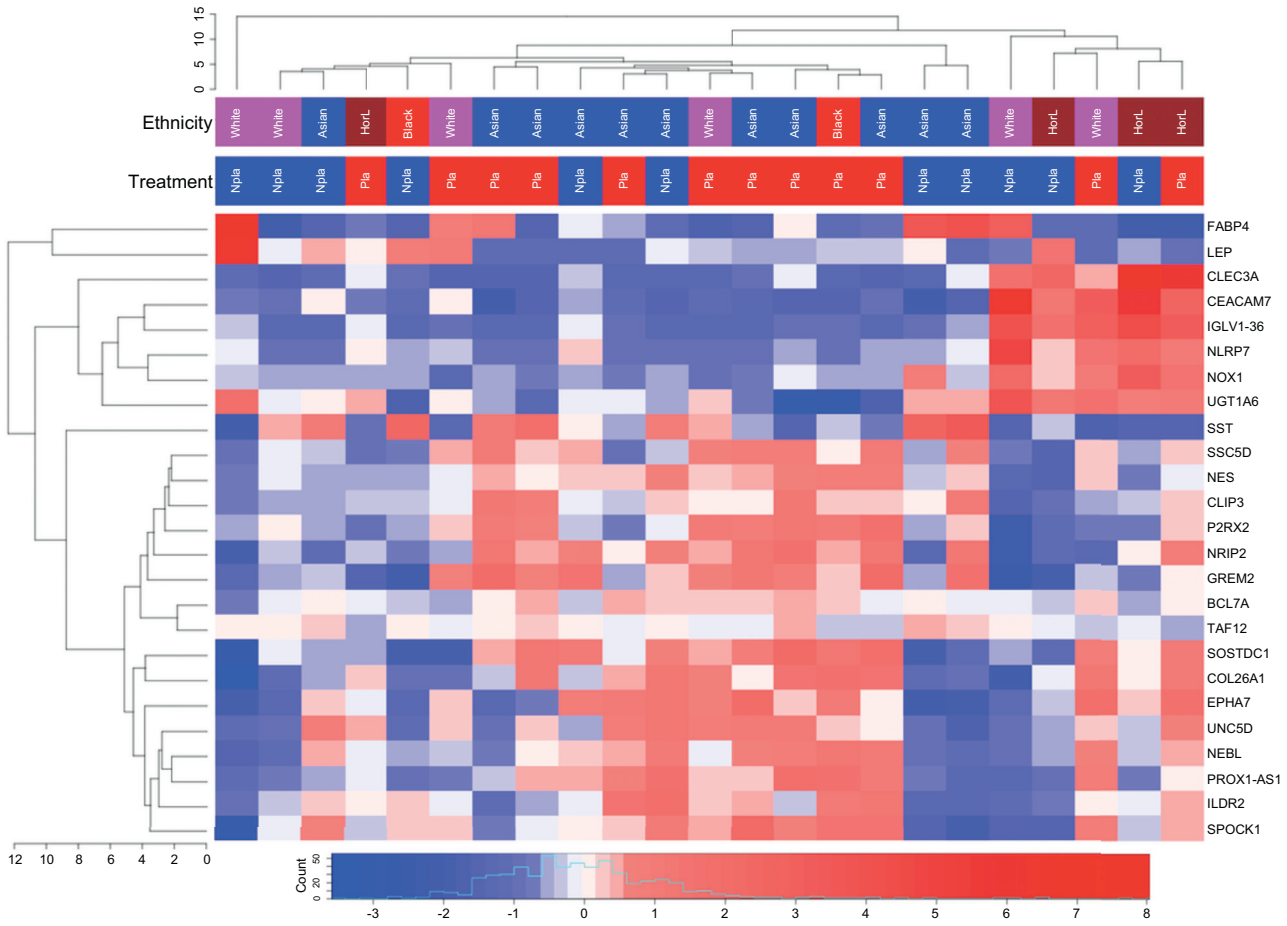

Figure 1 | Clustering heatmap of differentially expressed genes between Randall's plaque and non-Randall's plaque papilla tissues. There are 25 genes differentially expressed between Randall's plaque and nonplaque papilla tissue. The top 2 rows show categories of patient ethnicity and papilla tissue obtained by cold-cup biopsy. Ethnicity: pink, white; blue, Asian; brown, HorL (Hispanic or Latino); red squares, Black. Treatment: Pla (red squares), Randall's plaque tissue; Npla (blue squares), non-Randall's plaque tissue.

expressed genes (FDR < 0.01) were found between the papilla versus cortex, papilla versus medulla, and medulla versus cortex, respectively. Cluster analysis demonstrated patterns of gene expression among the papilla, medulla, and cortex that distinguished these 3 regions from each other (Figure 2). Genes differentially expressed in the papilla compared with both the medulla and cortex are listed in Supplementary Table S2. IPA disease and function analysis of these gene sets demonstrated upregulation of genes related to urinary and renal disorders, granulocyte response, vascular smooth muscle cell–proliferation, dehydration, and renal calcification. Downregulation of genes related to carboxylic acid-lipid-fatty acid transport and urine osmolality was observed. Changes in FABP4 expression were consistently found in transport of fatty acid, lipid, and carboxylic acid as disease or functional annotations when comparing annotations with the previous analysis performed between plaque and nonplaque papilla tissue described previously (Table 4).

Overlay of RNA-Seq datasets identifies FABP4 as a common under-expressed gene in stone-forming renal tissue

To look for common pathway genes between the 2 sets of samples, we analyzed the 2 sets of RNA-Seq results by overlaying their datasets via IPA comparison analysis. Supplementary Figure S3 lists network analysis results from overlaying these 2 RNA-Seq studies. Two disease and functional annotations were most commonly seen resultant from both studies: lipid metabolism and small-molecule biochemistry. Of interest, the disease and function analyses of these 2 RNA-Seq datasets found that FABP4 was 1 molecule observed in common between these annotations. Although 5 differentially expressed genes were identified as common elements after overlaying these 2 RNA-Seq datasets (Supplementary Table S3), only FABP4 demonstrated the similar expression pattern of downregulation in both the plaque papilla biopsies as well as in the papilla compared with the medulla and cortex.

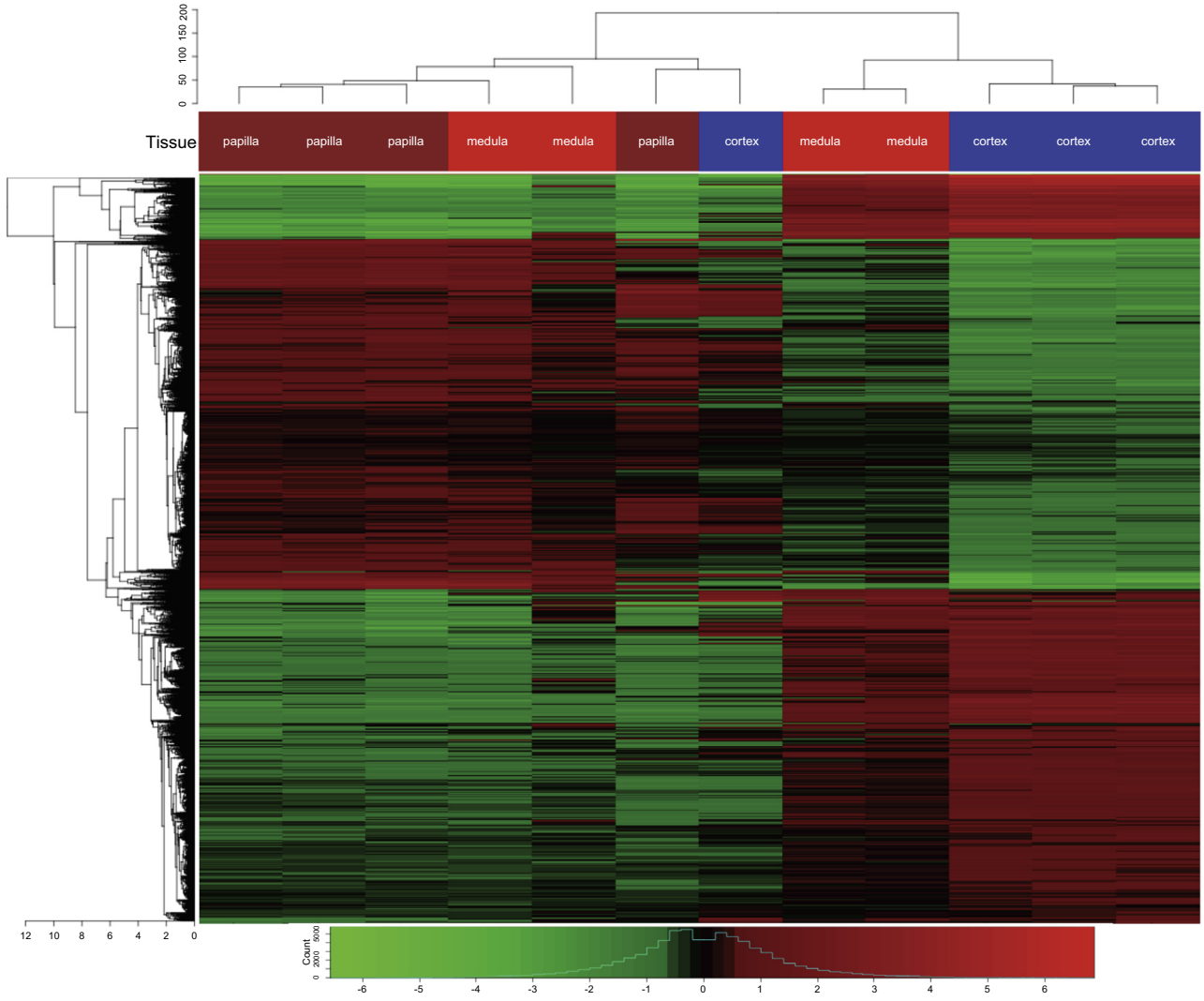

Figure 2| Clustering heatmap of differentially expressed genes among the papilla, medulla, and cortex regions of a kidney with severely recurrent calcium oxalate stones. The cluster trees demonstrate the result among all pairwise comparisons with regard to each tissue type. Tissue: brown squares, papilla; red squares, medulla; blue squares, cortex.

Table 4 | Disease and function analysis of differentially expressed genes in papilla compared with medulla and cortex region

Categories	Diseases or functions annotation	Activation *z* score[a]	*P* value	Number of molecules
Organismal injury and abnormalities, renal and urologic disease	Urination disorder	3.39	0.000005	18
Organismal injury and abnormalities, renal and urologic disease	Polyuria	2.98	0.000000	9
Organismal injury and abnormalities, renal and urologic disease	Hydronephrosis	2.62	0.000001	10
Cell-to-cell signaling and interaction	Response of granulocytes	2.60	0.000119	8
Cardiovascular system development and function, cellular development, cellular growth and proliferation, organ development, skeletal and muscular system development and function, tissue development	Proliferation of vascular smooth muscle cells	2.35	0.000878	9
Hematologic system development and function	Hematocrit of blood	2.24	0.000111	5
Neurologic disease	Movement disorders	2.22	0.000472	38
Organismal injury and abnormalities	Dehydration	2.22	0.000552	6
Organismal injury and abnormalities	Dehydration of mice	2.22	0.002640	5
Organismal injury and abnormalities, renal and urologic disease	Calcification of kidney	2.18	0.000008	5
Lipid metabolism, small-molecule biochemistry	Synthesis of leukotriene	2.17	0.003370	5
Cell-to-cell signaling and interaction, drug metabolism, molecular transport, small-molecule biochemistry	Secretion of norepinephrine	2.00	0.001320	4
Skeletal and muscular system development and function	Function of muscle	−2.11	0.000784	15
Lipid metabolism, molecular transport, small-molecule biochemistry	Transport of fatty acid	−2.16	0.003370	FABP4, 4 others
Renal and urologic system development and function	Osmolality of urine	−2.18	0.000009	7
Lipid metabolism, molecular transport, small-molecule biochemistry	Transport of lipid	−2.45	0.000045	FABP4, 13 others
Molecular transport	Transport of carboxylic acid	−2.54	0.000329	FABP4, 7 others
Cardiovascular-system development and function, organ development	Heart rate	−2.73	0.000006	17
Molecular transport	Transport of molecule	−3.49	7.15E−14	FABP4, 76 others

FABP4, fatty acid–binding protein 4.
[a]Activation *z* score is a statistical measure of the match between expected relationship direction from knowledge base and observed gene expression. A positive score shows the consistent relationship between them.

Imaging and histology of recurrent stone-former kidney tissue localizes regions of mineralization

The microstructure of renal papilla from the severely recurrent stone-forming kidney was studied to contextualize how gene-expression profile results related to cellular and mineral structure found from RNA-Seq analyses. Figure 3 shows a renal *en bloc* specimen, extending from the papilla to the middle of the cortex, and a core biopsy specimen from this excised kidney. Micro-computed tomography (CT) imaging showed that mineralization alongside the renal tubule and vessels increased in density from the medulla to the tip of the papilla (Figure 3d). Mineralization was particularly concentrated in the papilla region, with some condensed as tubular shapes (Figure 3e and f). Renal core biopsy specimen imaging showed similar mineralization patterns with tubular diameters ranging between 5 and 50 μm in the papilla regions. Although mineral deposits were concentrated in the papilla region, no mineralization was seen in the renal medulla or cortex (Figure 3g–i).

Figure 4 shows histologic examination of the same kidney. Masson's trichrome stain[13] revealed the presence of collagen fibers in the interstitial space, more predominant in the renal papilla and medulla compared with the cortex. von Kossa and hematoxylin and eosin (HE) stain demonstrated an area of calcium phosphate (CaP) deposition measuring larger than 50 μm in diameter in the interstitial space near the collecting ducts in the papilla, whereas CaP depositions in and near the distal tubules in the medulla were much smaller.

Human and murine tissue validate FABP4 expression correlated with mineralization

We hypothesized that FABP4 was associated with mineralization and RP, the precursors to the development of CaOx stones. To test this hypothesis, we performed FABP4 immunohistochemistry on human kidney samples and examined FABP4 gene expression patterns in a hyperoxaluric nephrocalcinosis mouse model.[14]

Immunohistochemistry staining of FABP4 from needle-core biopsy specimens from the patient with recurrent CaOx stone are shown in Figure 5a. Diffuse positively stained cells are present in the cortex, which includes not only proximal tubular cells but also interstitial and mesenchymal cells surrounding glomeruli. Distal tubular cells in the medulla and collecting duct epithelial cells in the papilla stained positively for FABP4, whereas no interstitial cells were seen in these locations with FABP4 staining present. To compare FABP4 expression levels between plaque papillae and nonplaque papillae, as well as confirm consistency of its expression in human kidneys, additional validation of FABP4 expression by immunohistochemistry using a second human kidney containing RP was performed (Figure 5b). Similar to the renal needle-core biopsy specimens, both tubular epithelial cells and interstitial and mesenchymal cells in this second kidney confirmed FABP4 expression in the cortex, whereas only tubular epithelial cells expressed FABP4 in the papilla and medulla. In addition, fewer FABP4-positive collecting duct epithelial cells were present in papilla with RP present.

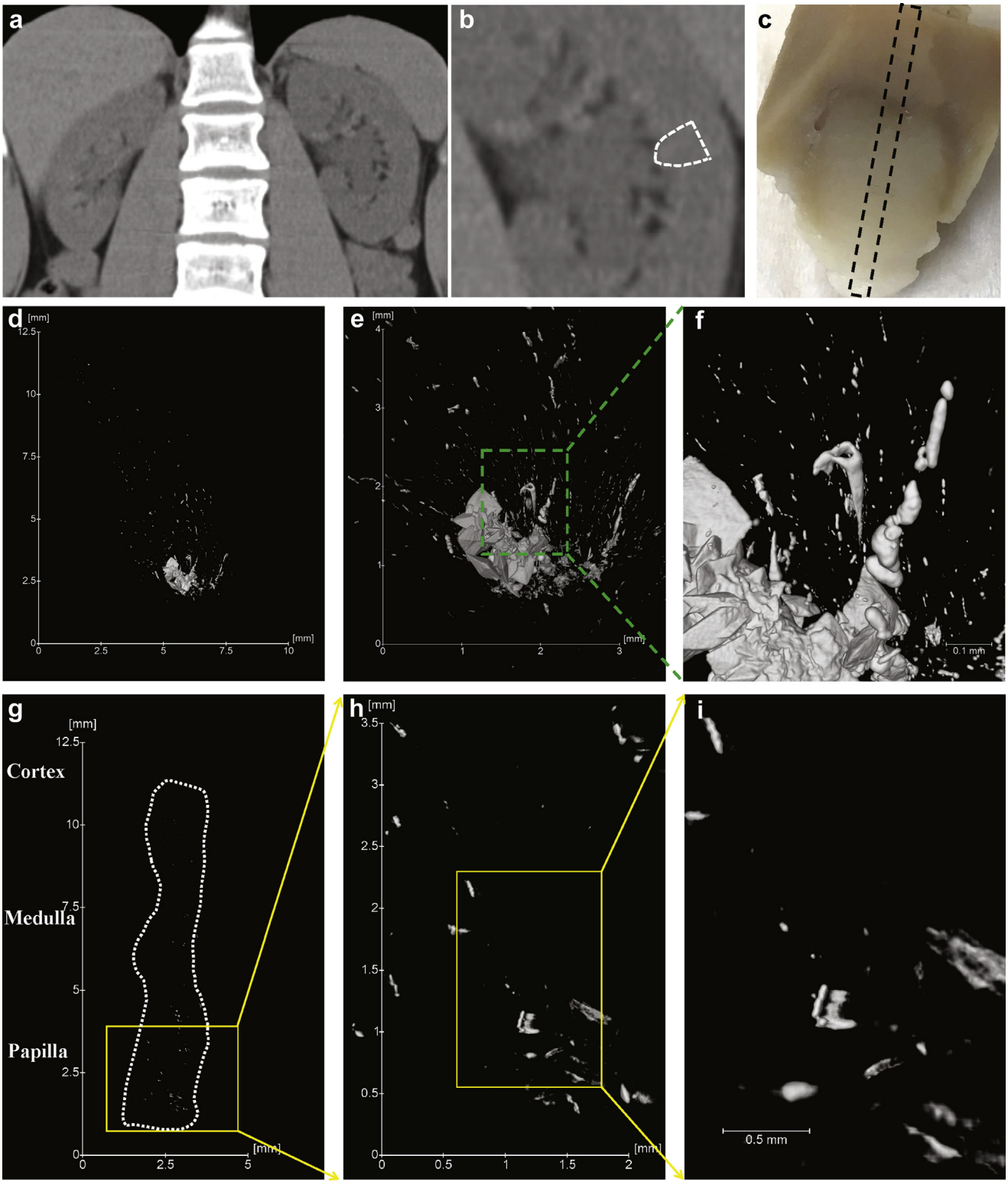

Figure 3 | Micro-computed tomography (CT) imaging of an *en bloc* and needle-core specimen of a severely recurrent calcium oxalate (CaOx) stone-forming kidney. (**a**) A clinical CT image shows both kidneys of the patient. (**b**) The white dashed line indicates the *en bloc* section of the left affected kidney excised for imaging after nephrectomy. (**c**) On removal of the *en bloc* specimen pictured, a core-needle biopsy was taken, with the black dashed line demonstrating the direction and depth of the needle-core biopsy taken. (**d–f**) Representative photographs demonstrate mineralization detected by micro-CT imaging of the entire papilla (**d**, original magnification ×4), in the distal part of the papilla (**e**, original magnification ×10), and around the tubules (**f**, original magnification ×20). (**g–i**) Representative photographs demonstrate mineralization detected by micro-CT imaging of the needle-core specimen biopsied from papilla through the cortex lesion (**g**, entire core specimen described as a surrounding dotted line; **h** and **i**, focused areas in the papilla). Micro-CT imaging demonstrates that the presence of mineralization was dominant in papilla areas of a needle-core biopsy specimen. Each horizontal bar describes a scale bar for each photograph.

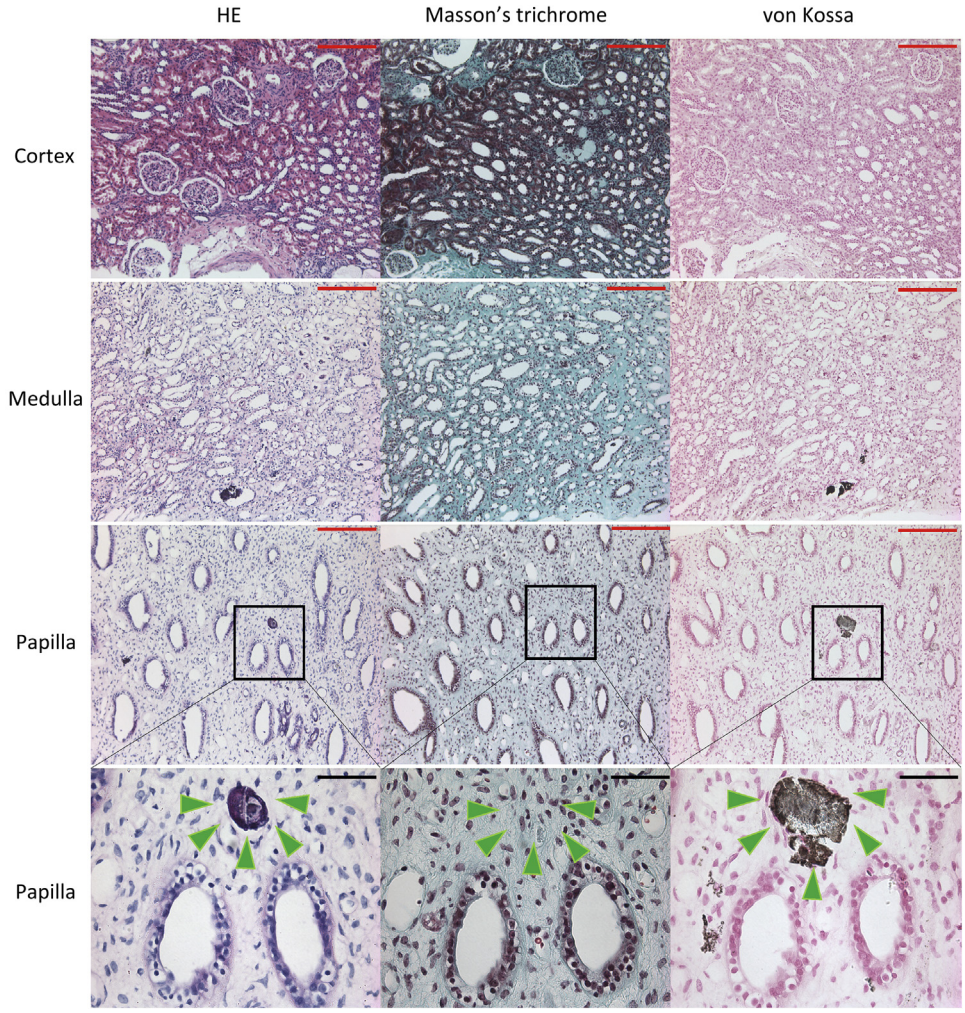

Figure 4 | Histology of specimens obtained by needle-core biopsy from a severely recurrent stone-forming kidney. Three different regions from this kidney were examined by hematoxylin and eosin (HE), Masson's trichrome, and von Kossa stains. The upper 3 rows represent stained samples at original magnification ×10 (red bars = 500 μm), whereas the bottom row shows a magnified view of the demarked insets of the renal papilla (original magnification ×400, black bars = 50 μm). There are calcium-phosphate deposits (arrowheads) in the interstitial space in close proximity to the collecting ducts and a substantial amount of collagen fibers (detected as a blue lesion by Masson's trichrome stain) surrounding areas of calcifications, consistent with the presence of Randall's plaques. To optimize viewing of this image, please see the online version of this article at www.kidney-international.org.

In a previously described CaOx nephrocalcinosis mouse model,[14] renal crystal deposition was seen in corticomedullary lesions, and the amount of crystal deposition in each kidney was the greatest on day 6 of treatment (Figure 6).[15] Microarray analysis of whole kidney tissue taken from mice killed at these treatment time points demonstrated that FABP4- expression levels decreased until day 6, which correlated negatively to the amount of renal crystal deposits seen by staining. The gene-expression level of secreted phosphoprotein 1 (Spp1) as mRNA of crystal matrix osteopontin was the highest on day 6. Expression for calcium-sensing receptor (Casr), vitamin D receptor (Vdr), and Klotho (Kl), all previously reported as urolithiasis-related molecules regulating calcium and phosphate metabolism,[16] were decreased in the presence of crystal deposition. Gene-expression levels of ADIPOQ and Cd68, which are coexpressed with FABP4,[17] were decreased and increased in the presence of crystal formation, respectively (Figure 6a). FABP4 levels were quantified as both protein and mRNA expression of FABP4 via immunohistochemical staining and quantitative polymerase chain reaction, respectively. These levels decreased as renal crystal deposition increased over time. Decreased levels of FABP4 expression were found in the tubule epithelial cells surrounding crystal deposits (Figure 6b).

Knockdown of FABP4 demonstrates increase of renal and urinary crystal depositions in a CaOx nephrocalcinosis mouse model

To examine the functional role of FABP4 on stone formation, we used a FABP4 knockout mouse treated with 6 days of intra-abdominal glyoxylate injection.

Polarized light microscopy demonstrated that Pizzolato-staining CaOx crystal depositions were mainly seen in the corticomedullary junction. A variety of sizes of octahedral

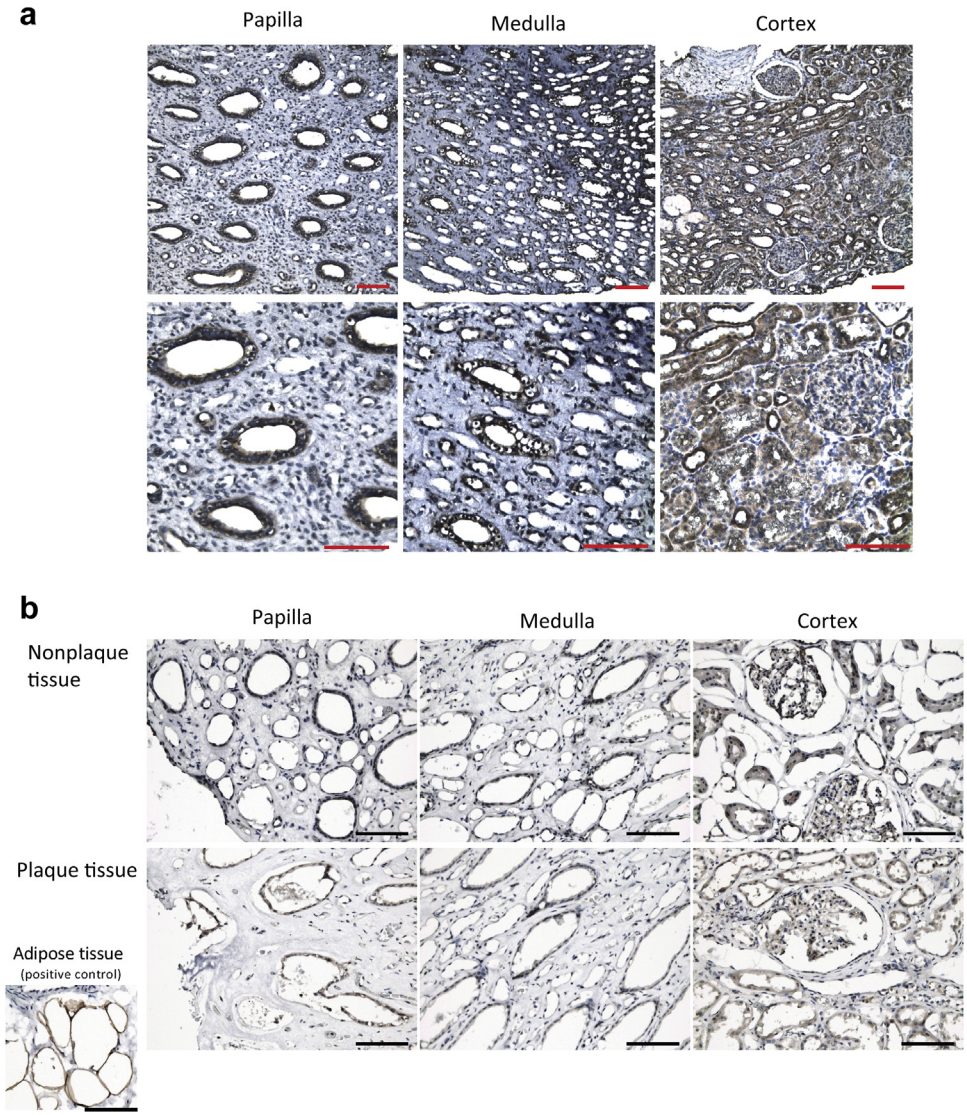

Figure 5 | Fatty acid–binding protein (FABP) 4 stain of a human kidney with calcium oxalate (CaOx) urolithiasis. (**a**) Staining of different areas from a needle-core biopsy specimen taken from a recurrent CaOx stone former. FABP4-positive stain cells were shown as dark brown with DAB color (Vector Laboratories, Burlingame, CA). Upper-row images demonstrate original magnification ×100, whereas lower-row images demonstrate original magnification ×200 (bars = 100 μm). (**b**) Staining of kidney tissue from a nephrectomy specimen with and without Randall's plaques present. FABP4-positive stain cells were shown as dark brown with DAB color. Original magnification ×200. Bar = 100 μm. Decreased intensity of FABP4 staining is seen in the papilla compared with the cortex regardless of whether plaques are present. Comparison between plaque and nonplaque-containing tissue samples demonstrates decreased amounts of FABP4-positive cells in papilla with plaque tissue (bottom row). To optimize viewing of this image, please see the online version of this article at www.kidney-international.org.

crystals were also seen in urine samples from these mice. Quantification revealed that the FABP4$^{-/-}$ animals had significantly larger amounts of renal crystal depositions and urinary crystal excretion compared with FABP4$^{+/+}$ mice (Figure 7a). Spp1, interleukin 6, and Cd68 gene expression in both mouse genotypes, as well as C-C motif chemokine 2 (Ccl2) expression in the FABP4$^{-/-}$ mouse increased with glyoxylate treatment. Ccl2 expression at day 6 was lower in the FABP4$^{-/-}$ mice compared with FABP4$^{+/+}$ mice (Figure 7b).

Serum and urinary measurements in these mice are summarized in Table 5. FABP4$^{-/-}$ mice had higher magnesium, oxalate, and citrate urinary excretion compared with FABP4$^{+/+}$ mice. Whereas glyoxylate treatment increased urinary phosphorus and oxalate excretion but decreased serum and urinary Ca and serum free fatty-acid levels, the FABP4$^{-/-}$ mice exhibited lower serum Ca levels and higher urinary volume compared with FABP4$^{+/+}$ mice.

DISCUSSION

Mounting evidence has linked obesity to urolithiasis for more than a decade, but—to our knowledge—no clear genetic etiology for this association has been presented to date.[18–20] Higher accumulation of visceral fat has been associated with an increased odds ratio for developing nephrolithiasis,[21] and a number of papers have reported the involvement of

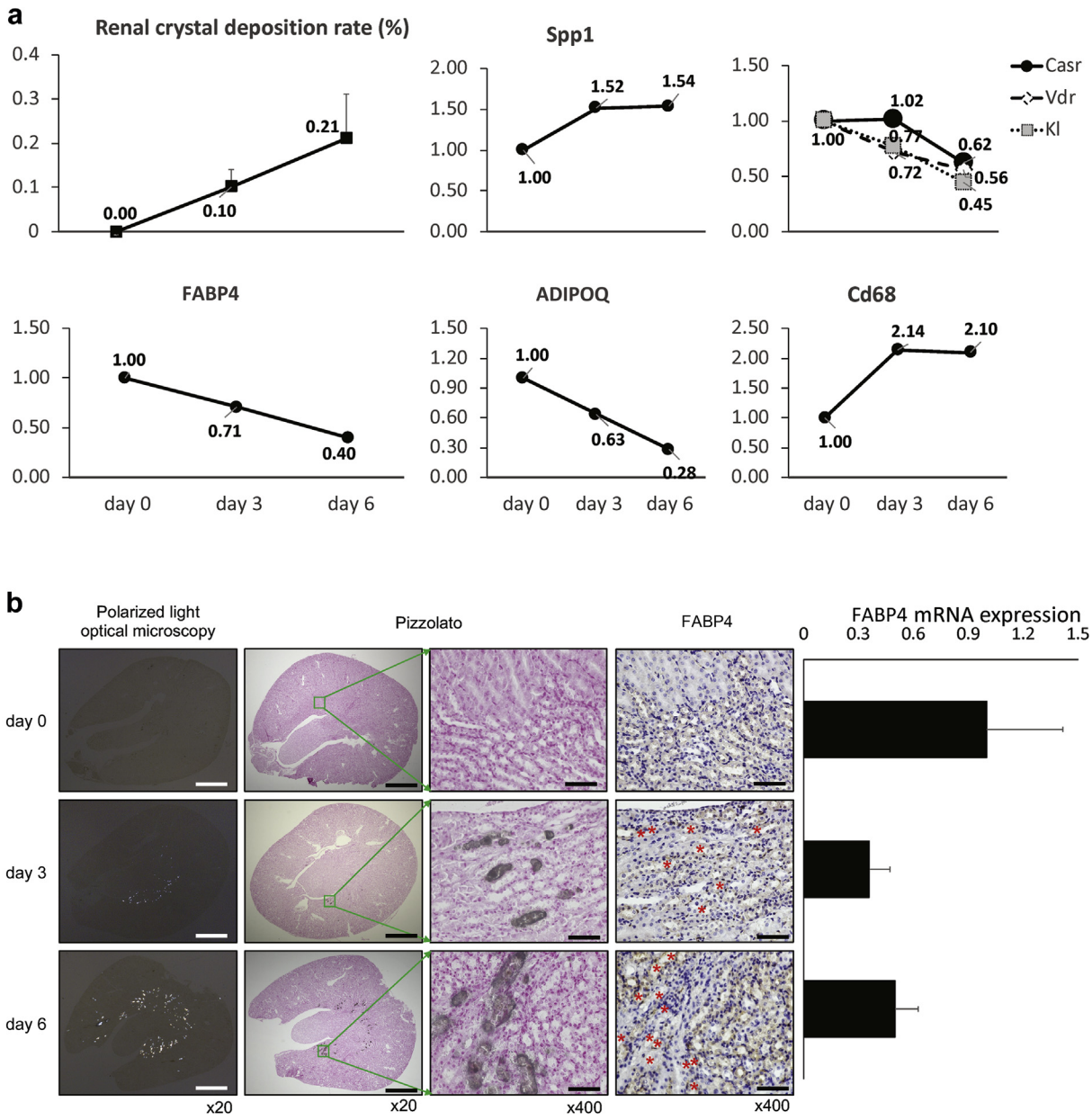

Figure 6 | Renal crystal deposition and DNA microarray expression patterns for fatty acid–binding protein (FABP) 4, and genes related to both nephrocalcinosis and FABP4 for hyperoxaluric stone model mice. (**a**) Quantification of renal crystal deposition rate demonstrates that there is the largest amount of crystal deposits present on day 6 of treatment. The gene expression level of FABP4 is lowest on day 6 in a normalized ratio. Similar to crystal deposition, the gene expression level of secreted phosphoprotein 1 (Spp1) as mRNA of the crystal matrix osteopontin, is the highest on day 6. Gene expression levels for calcium-sensing receptor (Casr), vitamin D receptor (Vdr), and Klotho (Kl), all of which have been reported as urolithiasis-related molecules regulating calcium and phosphate metabolism, decreased in the presence of crystal formation. Gene expression levels of ADIPOQ and Cd68, which are known to be related to FABP4 expression, were decreased and increased in the presence of crystal formation, respectively. (**b**) Polarized microscopic images of kidney sections are shown after daily intra-abdominal administration of glyoxylate in hyperoxaluric mice (first column of images). Intratubular calcium oxalate crystal deposits develop in the corticomedullary areas of the kidney, demonstrated by Pizzolato staining (second and third columns of images). Both FABP4 protein and mRNA expression are illustrated using immunohistochemical staining and quantitative polymerase chain reaction, respectively (fourth and fifth columns). There is decreased FABP4 expression in the tubule epithelial cells surrounding crystal deposits. Red asterisks, locations of crystal deposits. Magnifications are shown at the bottom of each microscopic image. Bars = 1 mm (2 left panels), 50 μm (2 right panels). To optimize viewing of this image, please see the online version of this article at www.kidney-international.org.

adipose cells with the formation of kidney stones.[22,23] The existence of adipocytes appears to accelerate CaOx crystal attachment to renal tubular epithelial cells by transwell coincubation via upregulation of inflammatory adipocytokine expression. Obese model rats[24,25] and mice[26] have demonstrated significantly larger amounts of renal crystal deposition compared with lean controls. These studies are mostly associative in nature, however, and few mechanistic pathways

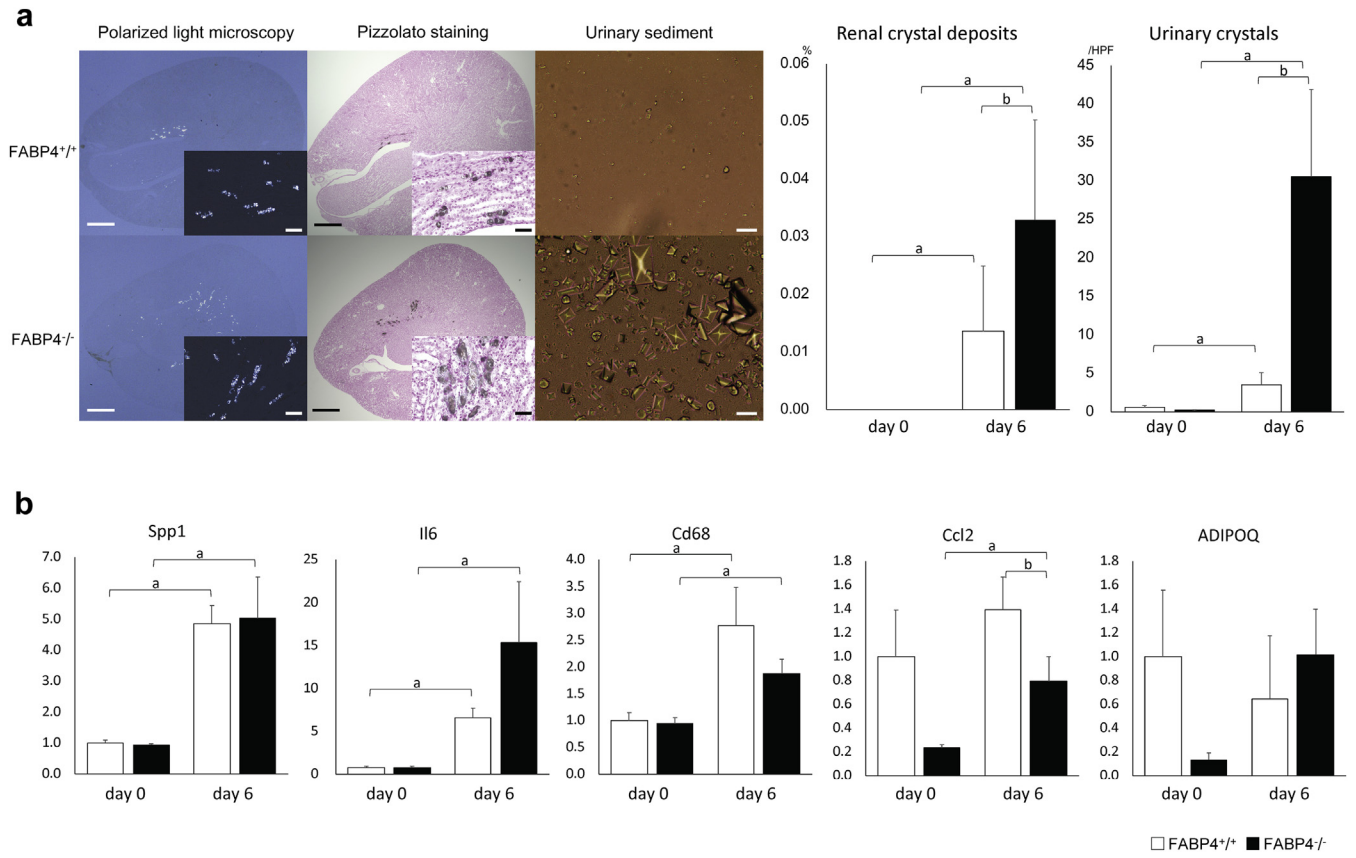

Figure 7 | Renal and urinary crystal deposition and nephrolithiasis-related gene expression patterns in fatty acid–binding protein (FABP) 4 knockout mice treated by intra-abdominal glyoxylate injection to drive calcium oxalate (CaOx) crystal deposition. (**a**) Polarized light microscopy and Pizzolato staining shows renal crystal depositions are mainly seen in the corticomedullary junction of both wild-type and knockout mice at day 6 of glyoxylate treatment. Different sizes of octahedral crystals are observed in urinary sediment samples at the same time points. The bar graphs illustrate that FABP4 deficiency leads to significantly larger amounts of renal crystal depositions and urinary crystal excretion. Quantification was performed by measuring crystal deposition area in the kidneys as well as counting the number of crystals present in several randomly selected lesions in the microscopic field of view of urine samples for each mouse. Samples were collected on days 0 ($n = 6$) and 6 ($n = 14$) for analyses. Original magnification ×20; inset, original magnification ×400. Bars = 0.5 mm; inset bars = 50 μm. Data are presented as mean ± SE. (**b**) Quantitative polymerase chain reaction shows gene expression levels of secreted phosphoprotein 1 (Spp1), interleukin 6 (Il6), and Cd68 in both mouse genotypes as well as C-C motif chemokine 2 (Ccl2) in the FABP4$^{-/-}$ mouse increased at day 6 of glyoxylate treatment. In addition, the Ccl2 expression at day 6 was lower in the knockout compared with the wild-type mice. [a]Significant differences compared with day 0 of glyoxylate administration at $P < 0.05$. [b]Significant differences between the FABP$^{+/+}$ and FABP$^{-/-}$ mice at $P < 0.05$. Each gene's expression was normalized to the expression of β-actin for internal control. To optimize viewing of this image, please see the online version of this article at www.kidney-international.org.

connecting obesity to kidney stones have been fully elucidated.

In this study, we took a transcriptomics approach to identify new mechanisms by which urinary stones form. The genetic basis for the formation of CaOx stones has remained shrouded in mystery despite the high prevalence and recurrence rate for NL. Previous studies in NL have relied on microarray analyses, and we apply RNA-Seq approaches in urinary stone disease for the first time. Our approach was unique in that our ability to access renal tissue from patients with NL in multiple ways provided 2 types of rare transcriptomic datasets: namely, renal papilla biopsy tissue from multiple patients with stones of varying types with and without RP as well as a whole kidney from 1 patient with severely recurrent kidney stones. Thus, we were able to compare 2 transcriptomic datasets that not only surveyed many patients with renal calcification but also different locations within a single severely affected kidney to contextualize the anatomic locations important for stone formation. The overlay of these 2 RNA-Seq datasets revealed associations between FABP4 downregulation, adipogenesis, and RP formation in NL. The importance of FABP4 as a functional gene was supported by immunohistochemistry staining of renal tissue. Taking human transcriptomic data back to a vertebrate model in the form of microarray data from kidneys of a stone-forming mouse model validated that FABP4 expression levels were decreased during the development of renal crystal deposition. Moreover, functional studies with a FABP4 knockout mouse revealed this gene deficiency leads to development of both renal and urinary crystals, which was consistent with our human and CaOx nephrocalcinosis model mouse results. In total, we present transcriptomic,

Table 5 | Serum and urinary variables in FABP4$^{+/+}$ and FABP$^{-/-}$ mice

	Glyoxylate treatment, day 0		Glyoxylate treatment, day 6	
	FABP$^{+/+}$	FABP$^{-/-}$	FABP$^{+/+}$	FABP$^{-/-}$
Serum				
Creatinine, mg/dl	0.12 (0.08)	0.13 (0.02)	0.12 (0.03)	0.12 (0.03)
Blood urea nitrogen, mg/dl	26.58 (7.40)	28.73 (1.25)	39.85 (18.22)	37.71 (13.76)
Ca, mg/dl	9.92 (0.56)	9.57 (0.34)	9.11 (0.48)[a]	8.66 (0.55)[a,b]
P, mg/dl	6.00 (1.35)	7.05 (0.67)	7.36 (0.93)	6.77 (0.78)
Mg, mg/dl	3.12 (0.41)	3.13 (0.28)	2.91 (0.40)	2.94 (0.38)
Na, mEq/l	144.33 (1.63)	145.33 (1.75)	149.00 (4.33)[a]	145.71 (6.32)
Total cholesterol, mg/dl	76.00 (19.78)	81.17 (8.28)	103.64 (17.63)[a]	91.64 (20.06)
Triglyceride, mg/dl	60.00 (32.67)	46.83 (10.46)	38.79 (26.75)[a]	52.36 (20.32)
Free fatty acids, mg/dl	0.78 (0.18)	0.72 (0.15)	0.47 (0.17)[a]	0.54 (0.14)[a]
Urine				
Volume, ml	1.50 [1.25, 1.60]	1.80 [1.80, 1.95]	1.30 [0.85, 1.48]	2.80 [2.35, 3.30][a,b]
pH	6.75 [6.12, 7.00]	6.25 [6.00, 6.50]	6.00 [6.00, 6.88]	6.00 [6.00, 8.00]
Ca, μmol· g^{-1}· Cr^{-1}	15.2 [13.3, 23.1]	12.0 [7.3, 15.0]	5.90 [3.27, 8.46][a]	5.13 [2.60, 7.30][a]
P, μmol· g^{-1}· Cr^{-1}	54.4 [42.3, 81.5]	100.0 [85.8, 132.8]	136.3 [118.8, 200.3][a]	187.5 [164.3, 195.2][a]
Mg. μmol· g^{-1}· Cr^{-1}	67.6 [64.0, 69.1]	101.2 [96.3, 103.8][b]	48.2 [11.9, 77.8]	48.0 [0.64, 73.6][a]
Na, μmol· g^{-1}· Cr^{-1}	357 [327, 371]	383 [363, 387]	432 [388, 494]	377 [336, 458]
Oxalate, μmol· g^{-1}· Cr^{-1}	4.25 [3.32, 6.14]	7.13 [6.78, 7.78][b]	12.25 [7.43, 13.98][a]	12.04 [11.03, 16.75][a]
Cit, μmol· g^{-1}· Cr^{-1}	84.0 [74.6, 97.9]	114.1 [112.3, 117.7][b]	81.6 [50.9, 90.4]	66.4 [61.1, 76.1][a]

Ca, calcium; Cit, citrate; Cr, creatinine; FABP4, fatty acid–binding protein 4; Mg, magnesium; Na, sodium; P, phosphorus.
[a]Significant differences compared with the day 0 of glyoxylate administration at $P < 0.05$.
[b]Significant differences between the FABP$^{+/+}$ and FABP$^{-/-}$ mice at $P < 0.05$.
Values are presented as mean (SD), or median [interquartile range].

morphologic, and *in vivo* analyses highly suggestive that decreasing FABP4 expression is linked to development of RP, resulting in the formation of CaOx stones.

The formation of RP is believed to be a fundamental step for stone formation. Despite limited sample numbers, our analysis identified FABP4 as a key gene directly associated with CaOx lithogenesis. FABP4 is a member of the family of cytoplasmic FABPs and mainly expressed in adipocytes and macrophages, whereas ectopic expression has been reported in the kidney.[27,28] FABP4 was detected in peritubular capillary endothelial cells in both the cortex and the medulla but not in glomerular or arterial endothelial cells under normal conditions.[29] Tanaka *et al.* also reported FABP4 is expressed not only in peritubular capillary cells but also in glomerular and tubular epithelial cells in patients with lupus nephritis, IgA, and diabetic nephropathy.[30] In our study, FABP4 protein expression was predominant in the cortex followed by the medulla and papilla. FABP4 expression was demonstrated in glomerular and endothelial cells in the interstitial space, most notably in the cortex. Since papilla and RP tissue exhibited decreased FABP4 expression in their tubular cells and other cells of the interstitial space, we believe decreased FABP4 expression in a gradient from the cortex through the papilla contributes to the formation of RP in the tip of papilla.

FABP4 expression is induced during adipocyte and macrophage differentiation, and its mRNA is regulated by fatty acids, peroxisome proliferator-activated receptor (PPAR) γ agonists, dexamethasone, and insulin.[17,28] Some studies have also reported that polymorphisms of FABP4 are related to insulin resistance, a risk factor for diabetes.[31,32] Interestingly, our previous studies have demonstrated that administration of pioglitazone, a PPAR γ agonist, suppresses renal crystal deposition via anti-inflammatory and oxidative stress effects in hyperoxaluric stone-forming rats.[33,34] This current study demonstrates that FABP4$^{-/-}$ mice had lower Ccl2 expression at day 6 of glyoxylate treatment despite others showing that FABP4-deficient mice display an uncompromised phenotype under normal physiological conditions.[28] Previous studies have reported that FABP4 may affect macrophage activity by increased Ccl2 protein secretion.[35] FABP4 deficiency could result in dysregulation of macrophage function, leading to accelerated crystal formation, as we have reported previously.[36]

As a novel therapeutic target for NL treatment, there are several clinical implications for our findings. Secreted FABP4 levels may serve as a marker or therapeutic target for renal diseases.[37–42] Circulating serum FABP4 levels have been associated with worsened renal dysfunction in patients with diabetes mellitus,[37,38] a history of cardiovascular events, decreased glomerular filtration rate,[40] or on chronic hemodialysis.[39] In addition, urinary FABP4 levels correlate with severity of albuminuria, yearly decrease of glomerular filtration rate in healthy volunteers,[41] and prevalence of pediatric kidney stones.[42] Similar to other FABP4 studies for cardiovascular disease,[43] these studies suggest that upregulation of FABP4 is a risk factor and biomarker for the development of renal disease. On the contrary, we found that both mRNA and protein expression levels of FABP4 were downregulated in papillae with RP, which are considered to be in a pre–stone-forming state in the kidney. Most importantly, our study revealed FABP4 deficiency caused CaOx crystal development in both kidneys and urine of nephrocalcinosis model mice. Although the FABP4 knockout mice showed a few mineral composition differences from wild-type mice, such as slight

increase of urinary oxalate and citrate excretion at baseline as well as less serum Ca level after glyoxylate treatment, the heterogeneity of this biochemical data may not be enough to support the existence of *in vivo* metabolic difference between these 2 phenotypes. In this context, we speculate that based on this cumulative evidence,[7,44,45] impairment of transporting fatty acid could cause both interstitial and tubular epithelial cell damage and macrophage dysfunction, resulting in a transition from apoptosis to mineral deposition. Further functional analysis studies of FABP4 on a tissue-specific level should be conducted to better understand these mechanisms.

We recognize some limitations of this current study. First, as both RNA-Seq datasets had limited numbers of samples from calcium stone formers, the results of our study may not represent the gene-expression profile of all kidney stone formers. We used tissue from subjects with either pure or primary component CaOx stones to make the tissue sources as homogenous as possible, but these may still represent a heterogeneous group. Second, sample-collection bias for papillary tissue biopsies may have affected the data analyses. Biopsy forceps are small instruments, and their control is not completely precise. For samples obtained from a plaque area, some nonplaque tissue might have been included and *vice versa*. On a cellular level, these differences may have been enough to induce some heterogeneity. Third, ideal control samples would have included renal tissue taken from non–stone-forming healthy kidneys. We were unable to include these types of samples, as obtaining normal kidney specimens from healthy subjects is extremely challenging.

Taken together, our data revealed impairment of lipid metabolism in papillae with RP tissue and downregulation of FABP4 associated with plaque formation. Immunohistochemistry of human kidney specimens and experiments of nephrocalcinosis model mice and FABP4 knockout mice validated FABP4 downregulation as an important feature of papillary plaques and the formation of stones in the kidney. FABP4 appears to be a key molecule for the formation of kidney stones and may prove to be a therapeutic target for their prevention.

METHODS

Gene expression profiles differ in stone-forming regions of renal papilla tissue

Patients. This was a prospective multicenter transcriptomics study, conducted at 2 institutions: Nagoya City University and University of California, San Francisco. Institutional Review Board (IRB) approvals were obtained from the 2 coordinating sites: Nagoya City University (No. 929) and University of California, San Francisco (CHR 14-14533). During the study period between April 2015 and August 2016, renal papillary biopsies were performed in consecutive patients with either pure or predominantly CaOx stones. Included were all patients aged 18 and above, with upper urinary tract stones requiring ureteroscopy or percutaneous nephrolithotomy for stone removal, who were able to provide written consent to participate. Excluded were patients who were pregnant, previously diagnosed with cancer, had evidence of active urinary tract infection, or systemic disease likely to lead to death within 5 years. Patients with renal units displaying complex anatomy of the upper urinary tract, severe hydronephrosis, or complete staghorn stones were also excluded.

Endoscopic renal papilla biopsy

After complete stone removal was achieved, we obtained renal papillary tissue from upper and middle calyces using BIGopsy Backloading Biopsy Forceps (Cook Medical Incorporated, Bloomington, IN). Both RP and normal-appearing papilla tissues were biopsied to compare their RNA profiles.[46]

Renal papilla tissue demonstrates distinctive gene expression patterns compared with the medulla and cortex

Patient. Specimens were obtained from a 23-year-old man with severe recurrent CaOx stones of the left kidney, with associated debilitating pain. After failing conservative therapy and undergoing an informed discussion, the patient underwent laparoscopic left nephrectomy, and the kidney specimen was removed intact. Institutional review board approval for tissue analysis was obtained as part of a prospective data registry study[47] (CHR 14-14533).

Needle-core biopsy of removed left kidney

After removal of the specimen from the body, 4 needle-core specimens were taken using a biopty gun (Bard Medical, Covington, GA), directed from the capsule toward each papilla tip (Supplementary Figure S2). Each core biopsy specimen was between 2.5 and 3.0 cm in length. Each core was divided into 3 equal-length samples, representing the papilla, medulla, and cortex (n = 4 for each).

En bloc resection of removed left kidney

The removed kidney from this same patient was used for micro-CT imaging. One papilla surrounded by medulla and cortex was excised by a scalpel as an *en bloc* specimen, then preserved in formalin for imaging.

RNA extraction for both cold cup biopsied papilla tip and needle-core biopsied renal tissue

We have previously described the RNA extraction protocol used.[46]

RNA-sequencing

RNA-Seq libraries were generated using 1 ng of total RNA and the Ovation RNA-Seq System V2 and Ultralow Library Construction System sample prep kits (NuGeneration Ltd, Manchester, UK). Libraries were multiplexed at a density of 4 per flow-cell lane and sequenced on the HiSeq 4000 (Illumina Inc, San Diego, CA) to generate single end 50-bp reads per the manufacturer's instructions. Data analysis was performed by DESeq2 (Bioconductor, Fred Hutch, Seattle, WA)[48] for differential expression comparison and IPA for causal network analysis, as previously reported.[7,16] Data were first adjusted for ethnicity, using a linear model, then tested specifically for the plaque versus nonplaque condition, using a Wald test. All data were deposited in Gene Expression Omnibus (GSE116860).

Obtaining human kidney tissue including RP formation for validation of FABP4 expression

In an institutional review board–approved study (CHR 14-14533), a radical nephrectomy specimen for renal tumor was sectioned to isolate the corticomedullopapillary complex in grossly normal appearing kidney tissue, sufficiently distant from the malignancy in question. The patient had no history of stone disease. RP was

confirmed by micro-CT to determine the area used for immunohistochemistry.

Histology
Slices of 10% formalin-preserved renal sections from the RP group were examined by HE, Masson's trichrome, von Kossa, and Pizzolato staining, as described previously.[7]

Immunohistochemical staining
Immunohistochemistry for FABP4 was performed on 4-μm–thick sliced biopsy sections with Anti-FABP4 rabbit polyclonal antibody (Abcam, Cambridge, UK), secondary antibody kits (Vector Laboratories, Burlingame, CA), and DAB substrate kit (Vector Laboratories), according to the manufacturer's instructions.

Micro-CT imaging
The specimens were placed in a centrifuge tube in 50% ethanol and mounted inside a calibrated micro-CT unit, then imaged for analyses, as described previously.[49]

Microarray analysis for CaOx nephrocalcinosis mice model
All animal studies followed the recommendations of the National Institutes of Health (NIH) and the Nagoya City University Guide for the Care and Use of Laboratory Animals. Eight-week-old male C57BL/6N mice (n = 18) were given an intraabdominal injection of 80 mg/kg of glyoxylate for 12 days, and renal tissues were collected for analyses.[14] Details of the microarray analysis were described in a previous report.[15]

FABP4 transgenic mouse model
C57BL/6J-aP2$^{-/-}$ (FABP$^{-/-}$) mice[50] were donated by Sapporo Medical University and Harvard University. Mice were given daily intraabdominal injections of 80 mg/kg glyoxylate to drive stone formation. Kidneys, blood, and 24-hour urine samples were collected[14] on days 0 (n = 6) and 6 (n = 14) for analyses, as previously reported.[51]

Quantitative polymerase chain reaction
The primers used are listed in Supplementary Table S4. Quantitative polymerase chain reaction was performed using a TaqMan Fast Universal PCR Master Mix (4352042, Applied Biosystems, Waltham, MA) with a 7500 Fast RT-PCR System (Applied Biosystems).

Statistical analysis
Statistical analysis for RNA-Seq and microarray analyses were performed according to their analysis software specifications (DESeq2 and GeneSpring GX, respectively). The Fisher exact test was used to calculate statistical significance for overlap of our RNA-Seq dataset molecules, with molecule sets representing multiple annotations including canonical pathways, upstream regulators, and diseases. *P* values for the given functions were calculated by considering the number eligible for analysis within the dataset, the total number of molecules known to be associated with that annotation and that were in the selected reference set, the total number of molecules in the reference set, and the total number of molecules for analysis that did not match that annotation. Using these inputs, IPA causal pathway analyses were then used for our final output. Differences were considered statistically significant at $\alpha < 0.05$. All statistical analyses were performed using EZR for R (R project).[52]

DISCLOSURE
MLS and TC serve as paid speakers and consultants for Boston Scientific Corporation and have received educational grant funding from Richard Wolf. MLS has served as a paid speaker for the Karl Storz Company. All the other authors declared no competing interests.

ACKNOWLEDGMENTS
We thank Andrea Barczak, Rebecca Barbeau, and Walter L. Eckalbar from the University of California, San Francisco (UCSF) SABRE Functional Genomics Core Facility for assistance with RNA-sequencing and Linda Prentice from the UCSF Division of Biomaterials and Bioengineering, Department of Preventive and Restorative Dental Sciences at UCSF for support with histology.

This work was supported by the US National Institutes of Health with grants K12-DK-07-006 (TC), P20-DK-116193 (TC) and P20-DK-100863 (MLS, TC), as well as JSPS KAKENHI Grant #16K11054 (KT, TY), The Naito Foundation Research Grant (KT), and The Mochida Memorial Foundation for Medical and Pharmaceutical Research (KT). The sponsors played no direct role in the study.

SUPPLEMENTARY MATERIAL
Supplementary File (PDF)

Figure S1. Diseases and Functions networks determined by Ingenuity Pathway Analysis (IPA) for differentially expressed genes in renal papilla tissue containing Randall's plaques compared with non-Randall's plaque areas (false discovery rate < 0.1). Two networks are merged to show their functional relationship among these gene sets: Endocrine System Development and Function; Lipid Metabolism; Small Molecule Biochemistry (IPA score = 37); and Gastrointestinal Disease, Hepatic System Disease, Organismal Injury, and Abnormalities (IPA = score 18). Red shapes indicate upregulated mRNAs, whereas blue shapes indicate downregulated mRNAs. Different shapes and prediction outlines are indicated in the legend box.

Figure S2. Schema of needle-core biopsied specimens. A 16-gauge biopty gun (MAGNUM, Bard Medical, Covington, GA) punctured from the tip of the papilla through the medulla and to the middle of the cortex (left illustration). The middle stereoscopic photo represents an entire core specimen. The core specimen was divided into 3 equal-length parts, representing the papilla, medulla, and cortex (n = 4 for each region), then examined by further analyses, including RNA sequence and histology (black scale bar = 500 μm).

Figure S3. Overlapping networks between 2 RNA-sequence studies. (**A**) Venn diagram of 3 different comparisons from two RNA-sequence studies. Orange, blue, and green circles represent the comparison between plaque versus nonplaque papillary tissues, papilla versus medulla regions, and papilla versus cortex regions, respectively. The size of each circle corresponds to the total network score calculated by IPA. (**B**) Table summarizes the IPA results from overlaying the networks of the 2 RNA-sequence studies. Lipid Metabolism and Small-Molecule Biochemistry emerge as the top Disease and Function annotations among these networks.

Table S1. Genes expressed statistically (false discovery rate < 0.1) differentially between plaque and nonplaque papilla tissue.

Table S2. Genes differentially expressed in the papilla compared with both the medulla and cortex.

Table S3. Differentially expressed genes overlapping between 2 RNA-sequence studies.

Table S4. TaqMan Probe information used for qPCR.

REFERENCES
1. Sorokin I, Mamoulakis C, Miyazawa K, Rodgers A, Talati J, Lotan Y. Epidemiology of stone disease across the world. *World J Urol*. 2017: 1–20.

2. Antonelli JA, Maalouf NM, Pearle MS, Lotan Y. Use of the National Health and Nutrition Examination Survey to calculate the impact of obesity and diabetes on cost and prevalence of urolithiasis in 2030. *Eur Urol*. 2014;66:724–729.
3. Lieske J. New insights regarding the interrelationship of obesity, diet, physical activity, and kidney stones. *J Am Soc Nephrol*. 2014;25:211–212.
4. Kohjimoto Y, Sasaki Y, Iguchi M, Matsumura N, Inagaki T, Hara I. Association of metabolic syndrome traits and severity of kidney stones: results from a nationwide survey on urolithiasis in Japan. *Am J Kidney Dis*. 2013;61:923–929.
5. Kum F, Mahmalji W, Hale J, Thomas K, Bultitude M, Glass J. Do stones still kill? An analysis of death from stone disease 1999-2013 in England and Wales. *BJU Int*. 2016;118:140–144.
6. Coe FL, Worcester EM, Evan AP. Idiopathic hypercalciuria and formation of calcium renal stones. *Nat Rev Nephrol*. 2016;12:519–533.
7. Taguchi K, Hamamoto S, Okada A, et al. Genome-wide gene expression profiling of Randall's plaques in calcium oxalate stone formers. *J Am Soc Nephrol*. 2017;28:333–347.
8. Hsi RS, Ramaswamy K, Ho SP, Stoller ML. The origins of urinary stone disease: upstream mineral formations initiate downstream Randall's plaque. *BJU Int*. 2017;119:117–184.
9. Wang Z, Gerstein M, Snyder M. RNA-Seq: a revolutionary tool for transcriptomics. *Nat Rev Genet*. 2009;10:57–63.
10. Zhao S, Fung-Leung W-P, Bittner A, Ngo K, Liu X. Comparison of RNA-Seq and microarray in transcriptome profiling of activated T cells. *PLoS One*. 2014;9:e78644.
11. Daga A, Majmundar AJ, Braun DA, et al. Whole exome sequencing frequently detects a monogenic cause in early onset nephrolithiasis and nephrocalcinosis. *Kidney Int*. 2017;93:204–213.
12. Gayral P, Weinert L, Chiari Y, Tsagkogeorga G, Ballenghien M, Galtier N. Next-generation sequencing of transcriptomes: a guide to RNA isolation in nonmodel animals. *Mol Ecol Resourses*. 2011;11:650–661.
13. Khan SR, Rodriguez DE, Gower LB, Monga M. Association of Randall plaque with collagen fibers and membrane vesicles. *J Urol*. 2012;187:1094–1100.
14. Okada A, Nomura S, Higashibata Y, et al. Successful formation of calcium oxalate crystal deposition in mouse kidney by intraabdominal glyoxylate injection. *Urol Res*. 2007;35:89–99.
15. Okada A, Yasui T, Hamamoto S, et al. Genome-wide analysis of denes related to kidney stone formation and elimination in the calcium oxalate nephrolithiasis model mouse: detection of stone-preventive factors and involvement of macrophage activity. *J Bone Miner Res*. 2009;24:908–924.
16. Taguchi K, Yasui T, Milliner DS, Hoppe B, Chi T. Genetic risk factors for idiopathic urolithiasis: a systematic review of the literature and causal network analysis. *Eur Urol Focus*. 2017;3:72–81.
17. Furuhashi M, Hotamisligil GS. Fatty acid-binding proteins: role in metabolic diseases and potential as drug targets. *Nat Rev Drug Discov*. 2008;7:489–503.
18. Taylor EN, Stampfer MJ, Curhan GC. Obesity, weight gain, and the risk of kidney stones. *JAMA*. 2005;293:455.
19. Yoshimura E, Sawada SS, Lee I-M, et al. Body mass index and kidney stones: a cohort study of Japanese men. *J Epidemiol*. 2016;26:131–136.
20. Lee S-C, Kim Y-J, Kim T-H, Yun S-J, Lee NK, Kim W-J. Impact of obesity in patients with urolithiasis and its prognostic usefulness in stone recurrence. *J Urol*. 2008;179:570–574.
21. Fujimura M, Sakamoto S, Sekita N, Mikami K, Ichikawa T, Akakura K. Visceral fat accumulation is a risk factor for urinary stone. *Int J Urol*. 2014;21:1184–1185.
22. Zuo L, Tozawa K, Okada A, et al. A paracrine mechanism involving renal tubular cells, adipocytes and macrophages promotes kidney stone formation in a simulated metabolic syndrome environment. *J Urol*. 2014;191:1906–1912.
23. Ichikawa J, Okada A, Taguchi K, et al. Increased crystal–cell interaction in vitro under co-culture of renal tubular cells and adipocytes by in vitro co-culture paracrine systems simulating metabolic syndrome. *Urolithiasis*. 2014;42:17–28.
24. Iba A, Kohjimoto Y, Mori T, et al. Insulin resistance increases the risk of urinary stone formation in a rat model of metabolic syndrome. *BJU Int*. 2010;106:1550–1554.
25. Sasaki Y, Kohjimoto Y, Iba A, Matsumura N, Hara I. Weight loss intervention reduces the risk of kidney stone formation in a rat model of metabolic syndrome. *Int J Urol*. 2015;22:404–409.
26. Fujii Y, Okada A, Yasui T, et al. Effect of Adiponectin on kidney crystal formation in metabolic syndrome model mice via inhibition of inflammation and apoptosis. *PLoS One*. 2013;8:e61343.
27. Storch J, McDermott L. Structural and functional analysis of fatty acid-binding proteins. *J Lipid Res*. 2009;50:S126–S131.
28. Furuhashi M, Saitoh S, Shimamoto K, Miura T. Fatty acid-binding protein 4 (FABP4): pathophysiological insights and potent clinical biomarker of metabolic and cardiovascular diseases. *Clin Med Insights Cardiol*. 2014;8:23–33.
29. Elmasri H, Karaaslan C, Teper Y, et al. Fatty acid binding protein 4 is a target of VEGF and a regulator of cell proliferation in endothelial cells. *FASEB J*. 2009;23:3865–3873.
30. Tanaka M, Furuhashi M, Okazaki Y, et al. Ectopic expression of fatty acid-binding protein 4 in the glomerulus is associated with proteinuria and renal dysfunction. *Nephron Clin Pract*. 2014;128:345–351.
31. Chan K-HK, Song Y, Hsu Y-H, You NY, F. Tinker L, Liu S. Common genetic variants in fatty acid–binding protein-4 (FABP4) and clinical diabetes risk in the Women's Health Initiative Observational Study. *Obesity*. 2010;18:1812–1820.
32. Mukamal KJ, Wilk JB, Biggs ML, et al. Common FABP4 genetic variants and plasma levels of fatty acid binding protein 4 in older adults. *Lipids*. 2013;48:1169–1175.
33. Taguchi K, Okada A, Yasui T, et al. Pioglitazone, a peroxisome proliferator activated receptor γ agonist, decreases renal crystal deposition, oxidative stress and inflammation in hyperoxaluric rats. *J Urol*. 2012;188:1002–1011.
34. Taguchi K, Okada A, Hamamoto S, et al. Differential roles of peroxisome proliferator-activated receptor-α and receptor-γ on renal crystal formation in hyperoxaluric rodents. *PPAR Res*. 2016;2016:1–11.
35. Bouquet J, Soloski MJ, Swei A, et al. Longitudinal transcriptome analysis reveals a sustained differential gene expression signature in patients treated for acute lyme disease. *mBio*. 2016;7:e00100–e00116.
36. Taguchi K, Okada A, Hamamoto S, et al. M1/M2-macrophage phenotypes regulate renal calcium oxalate crystal development. *Sci Rep*. 2016;6:35167.
37. Cabré A, Lázaro I, Girona J, et al. Plasma fatty acid-binding protein 4 increases with renal dysfunction in type 2 diabetic patients without microalbuminuria. *Clin Chem*. 2008;54:181–187.
38. Yeung DCY, Xu A, Tso AWK, et al. Circulating levels of adipocyte and epidermal fatty acid-binding proteins in relation to nephropathy staging and macrovascular complications in type 2 diabetic patients. *Diabetes Care*. 2009;32:132–134.
39. Sommer G, Ziegelmeier M, Bachmann A, et al. Serum levels of adipocyte fatty acid-binding protein (AFABP) are increased in chronic haemodialysis (CD). *Clin Endocrinol (Oxf)*. 2008;69:901–905.
40. Tönjes A, Kralisch S, Lössner U, et al. Metabolic and genetic predictors of circulating adipocyte fatty acid-binding protein. *Int J Obes*. 2012;36:766–773.
41. Okazaki Y, Furuhashi M, Tanaka M, et al. Urinary excretion of fatty acid-binding protein 4 is associated with albuminuria and renal dysfunction. *PLoS One*. 2014;9:e115429.
42. Kovacevic L, Lu H, Caruso JA, Govil-Dalela T, Thomas R, Lakshmanan Y. Marked increase in urinary excretion of apolipoproteins in children with nephrolithiasis associated with hypercalciuria. *Pediatr Nephrol*. 2017;32:1029–1033.
43. Rodríguez-Calvo R, Girona J, Alegret JM, Bosquet A, Ibarretxe D, Masana L. Role of the fatty acid-binding protein 4 in heart failure and cardiovascular disease. *J Endocrinol*. 2017;233:R173–R184.
44. Yasui T, Okada A, Hamamoto S, et al. Pathophysiology-based treatment of urolithiasis. *Int J Urol*. 2017;24:32–38.
45. Taguchi K, Okada A, Hamamoto S, et al. Proinflammatory and metabolic changes facilitate renal crystal deposition in an obese mouse model of metabolic syndrome. *J Urol*. 2015;194:1787–1796.
46. Taguchi K, Usawachintachit M, Hamamoto S, et al. Optimizing RNA extraction of renal papilla biopsy tissue in kidney stone formers: a new methodology for genomic study. *J Endourol*. 2017;31:922–929.
47. Chang HC, Tzou DT, Usawachintachit M, et al. Rationale and design of the registry for stones of the kidney and ureter (ReSKU): a prospective observational registry to study the natural history of urolithiasis patients. *J Endourol*. 2016;30:1332–1338.

48. Huber W, Carey VJ, Gentleman R, et al. Orchestrating high-throughput genomic analysis with Bioconductor. *Nat Methods*. 2015;12:115–121.
49. Wiener SV, Chen L, Shimotake AR, Kang M, Stoller ML, Ho SP. Novel insights into renal mineralization and stone formation through advanced imaging modalities. *Connect Tissue Res*. 2018;59:102–110.
50. Hotamisligil GS, Johnson RS, Distel RJ, Ellis R, Papaioannou VE, Spiegelman BM. Uncoupling of obesity from insulin resistance through a targeted mutation in aP2, the adipocyte fatty acid binding protein. *Science*. 1996;274:1377–1379.
51. Taguchi K, Okada A, Kitamura H, et al. Colony-stimulating factor-1 signaling suppresses renal crystal formation. *J Am Soc Nephrol*. 2014;25:1680–1697.
52. Kanda Y. Investigation of the freely available easy-to-use software 'EZR' for medical statistics. *Bone Marrow Transplant*. 2013;48:452–458.